Journal of Neurochemistry

JOURNAL OF NEUROCHEMISTRY | 2015 | 135 | 643–658 doi: 10.1111/jnc.13257

REVIEW

Stochastic optical reconstruction microscopy (STORM) in comparison with stimulated emission depletion (STED) and other imaging methods

Johnny Tam* and David Merino†

*National Eye Institute, National Institutes of Health, Bethesda, Maryland, USA

†ICFO-Institut de Ciències Fotòniques, Mediterranean Technology Park, Castelledefels, Barcelona, Spain

Abstract

Stochastic optical reconstruction microscopy (STORM) and stimulated emission depletion (STED) microscopy are two super-resolution optical microscopy approaches that have rapidly gained popularity in recent years. Both modalities offer super-resolution imaging capabilities with the potential for imaging in multiple colors, three-dimensions, and the possibility to image in live cells. In this review, we focus on the specific advantages and disadvantages of each technique in the context of each other. STORM has been reported to achieve higher spatial resolution when compared to STED, but a lengthy acquisition may be required. STED utilizes relatively higher laser intensities, but is able to generate a super-resolution image immediately after acquisition without the need for any additional data processing. Ultimately, the choice between STORM and STED will depend not only on the specific application, but also on the users' ability to understand and optimize the various parameters ranging from sample preparation to image acquisition, which determine the quality of the final image.

Keywords: confocal, fluorescence microscopy, stimulated emission depletion, stochastic optical reconstruction microscopy, super resolution, total internal reflectance fluorescence.

J. Neurochem. (2015) **135**, 643–658.

Cover Image *for this issue: doi: 10.1111/jnc.12914.*

Fluorescence microscopy has revolutionized our ability to visualize life's processes, particularly within cells, which are densely packed with proteins, organelles, and other biological matter. To do so, the approach followed in fluorescence microscopy has been to select specific structures of interest for imaging, rather than imaging all of these components within the cell at the same time. This can be done using a growing library of available techniques for decorating subcellular targets of interest with fluorophores or fluorescent dyes. Signal generated by these fluorophores is then used to image that specific subcellular structure.

For over a century, Abbe's law was thought to have imposed a hard limit on the spatial resolution of a microscope. This seemed reasonable, since this resolution was comparable to the wavelength of light used to interrogate the sample. According to Abbe's law from classical optics, for a typical optical microscope, the highest achievable spatial resolution in the lateral and axial directions can be approximated by:

$$d_{x,y} = \frac{\lambda}{2\mathrm{NA}} \quad (1)$$

$$d_z = \frac{2\lambda}{\mathrm{NA}^2} \quad (2)$$

where $d_{x,y}$ is the resolution in the lateral direction, d_z is the resolution in the axial direction, λ is the wavelength of the excitation beam, and NA is the numerical aperture of the

Received December 29, 2014; revised manuscript received June 5, 2015; accepted July 15, 2015.

Address correspondence and reprint requests to Johnny Tam, National Eye Institute, National Institutes of Health, Bethesda, Maryland, USA. E-mail: johnny@nih.gov

Abbreviations used: GFP, green fluorescent protein; PALM, photoactivation localization microscopy; RESOLFT, reversible saturable optical fluorescence transitions; SMLM, single-molecule localization microscopy; STED, stimulated emission depletion; TIRF, total internal reflectance fluorescence; STORM, stochastic optical reconstruction microscopy.

microscope objective. The best resolution in a conventional microscope and visible light is achieved by means of short wavelengths ($\lambda \sim 488$ nm) and it is generally accepted to be at best ~180 nm in the lateral directions and ~ 500 nm in the axial direction. Conventional microscopy is unable to image structures smaller than the limit set by diffraction.

It is worth noting that there are some other techniques that have demonstrated resolutions in the nanometer scale. For example, there are near-field optical microscopy approaches such as near-field scanning optical microscopy (NSOM) (Betzig *et al.* 1986, 1988), which utilize nanosized mechanical tips to detect light at distances within one wavelength from the sample. However, images can only be obtained from the surface of the sample, which limits its applicability for cell biology. There are also non-optical techniques such as electron microscopy (Hayat 1974) and atomic force microscopy (Binnig *et al.* 1986), which can achieve resolutions that are orders of magnitude beyond those reported in conventional optical microscopy. However, these techniques are also subject to limitations. Electron microscopy requires very specific and invasive sample preparation, making it incompatible with *in-vivo* or live experiments. In the case of atomic force microscopy, the technique can only provide topological information of the surface of the sample, and therefore intracellular imaging is not possible.

Fluorescence-based far field optical microscopy (where far-field optical microscopy techniques refer to the detection of light at many wavelengths away from the sample, as opposed to previously mentioned near-field approach) is now established as a very versatile tool for biological applications. To date, many approaches have already been developed to improve the quality of the images that can be generated. Techniques such as deconvolution microscopy (Agard 1984) and confocal microscopy (Minsky 1988; Webb 1996) have demonstrated that it is possible to resolve objects that are slightly smaller than the diffraction limit, in the lateral dimension. Notably, techniques such as 4Pi (Hell and Stelzer 1992), I5M (Gustafsson *et al.* 1999), or selective plane illumination microscopy (Siedentopf and Zsigmondy 1902; Voie *et al.* 1993; Stelzer *et al.* 1995; Kumar *et al.* 2014), have been able to achieve images below the diffraction limit set by Abbe in the axial direction. Furthermore, this limit was also overcome in the lateral direction using structured illumination microscopy (Bailey *et al.* 1993; Gustafsson 2000, 2005; Hell 2007). Although these techniques can generate images with resolutions that are better than the limit set by Abbe's law, these are not typically considered to be super-resolution techniques, since they do not hold the potential to increase resolution without limit (Hell 2003).

Recent advances in far-field optical microscopy have demonstrated the ability to image well below the diffraction limit, approaching the nanometer-scale (Hell and Wichmann 1994; Gustafsson 2005; Betzig *et al.* 2006; Hess *et al.* 2006; Rust *et al.* 2006). In this article, we will focus on these more recent far-field optical microscopy techniques, which are collectively referred to as super-resolution microscopy.

There are many approaches for achieving super-resolution, each with its own technical intricacies. Most of these super-resolution approaches can be conceptually organized into two main families: single-molecule localization microscopy (SMLM) and reversible saturable optical fluorescence transitions (RESOLFT) microscopy. SMLM includes a large family of techniques which originated from three seminal papers that were published in the same year. These techniques include stochastic optical reconstruction microscopy (STORM) (Rust *et al.* 2006), photoactivation localization microscopy (PALM) (Betzig *et al.* 2006), and fluorescence photoactivation localization microscopy (fPALM) (Hess *et al.* 2006). All of these techniques are based on the precise localization of many individual fluorescent molecules with very high resolution to build an image point by point (this is enabled by experimental control over the fluorescent molecules which can be assigned to on or off states). This principle has subsequently been expanded to a number of related approaches, including dSTORM (Heilemann *et al.* 2008), GSDIM (Fölling *et al.* 2008), and many others (Oddone *et al.* 2014). The second large family of super-resolution techniques, RESOLFT (Hell 2009), is based on the use of reversible saturable optical transitions between fluorescent and non-fluorescent states to inhibit fluorescence in the sample in a controlled way (Hell 2003, 2004; Hell *et al.* 2004). The RESOLFT family includes techniques such as stimulated emission depletion (STED) microscopy, ground state depletion (GSD) microscopy (Hell and Kroug 1995), and saturated structured illumination microscopy (Gustafsson 2005).

In this review, we will focus on the specific aspects of STORM as a representative of SMLM, and STED as a representative of the RESOLFT family. Although the general principles are very similar across each of the individual members of the SMLM and RESOLFT families, there are slight differences in implementation which lead to considerations that are unique to each of them. With regards to the SMLM family, the focus of this review is on STORM, but it is important to note that it shares many similarities with PALM. At the time that both techniques were introduced, the key difference between STORM and PALM was that STORM utilized photoswitchable dyes which were introduced via immunostaining, whereas PALM utilized photoactivatable fluorophores which were endogenously expressed. This has led to subtle differences in the various protocols associated with each technique (e.g. specific methods for controlling the on/off behavior of fluorophores, quantitative analysis after data acquisition, or sample preparation, to name a few). Some of these differences are now blurred with advances in fluorophore technology and with the invention of other related SMLM techniques. In each section, we will focus the discussion on the unique

considerations related to the classical implementation of STORM; wherever possible, relationships to subsequent versions of STORM as well as to PALM and other related SMLM techniques will be discussed.

STORM and STED are among the most popular super-resolution techniques (Fig. 1). Proof of this lies in the significant achievements that these techniques have enabled. In particular, using STORM, acquisition of images showing the actin cytoskeleton in fixed cells with resolutions of 10 nm in the lateral direction and 20 nm in the axial direction have been reported (Xu *et al.* 2012). Another compelling example of the achievements reached using STORM was the discovery that actin and spectrin form a ring-like cytoskeletal structure in axons (Xu *et al.* 2013). In living cells, STORM has been used to image at resolutions of 30 nm in the lateral direction and 50 nm in the axial direction, at a temporal resolution of 1–2 s (Jones *et al.* 2011). In terms of multiple colors, STORM imaging has been demonstrated in fixed cells for up to five different colors (Tam *et al.* 2014b). In the case of STED microscopy, lateral resolutions of up to 6 nm have been reported using STED in diamond samples (Rittweger *et al.* 2009). However, in biological samples, ~40 nm of both lateral and axial resolution have been reported when combining STED with 4Pi microscopy (Schmidt *et al.* 2008), although 20 nm is the highest lateral resolution reported using STED on a biological sample (Donnert 2006). Furthermore, STED experiments have been carried out in the brain of a living mouse, showing images of neurons over extended periods of time with 70 nm lateral resolution (Berning *et al.* 2012).

Both STORM and STED have been used to reveal the nanoscale organization of different structures in cells (Fig. 2). In this review, we discuss the technical details behind STORM and STED related to relevant aspects of their implementation, with an emphasis on how the similarities and differences contribute to the advantages and disadvantages of each technique. We also comment on other super-resolution techniques that may be an alternative to overcome limitations present in STORM and STED.

Fluorophore control

STORM and STED are both based on the ability to control subsets of fluorophores that are forced to be non-fluorescent and other subsets that are forced to be capable of fluorescence. Whereas STORM utilizes a random approach for the assignment of fluorophores to non-fluorescent and fluorescent states, STED utilizes a targeted approach in which designated fluorophores are directly assigned to their appropriate states in specific areas of the sample. These strategies for controlling the fluorescence are critical for achieving super-resolution.

In the case of wide-field microscopy, all the fluorophores are imaged at the same time, and the resulting image is a

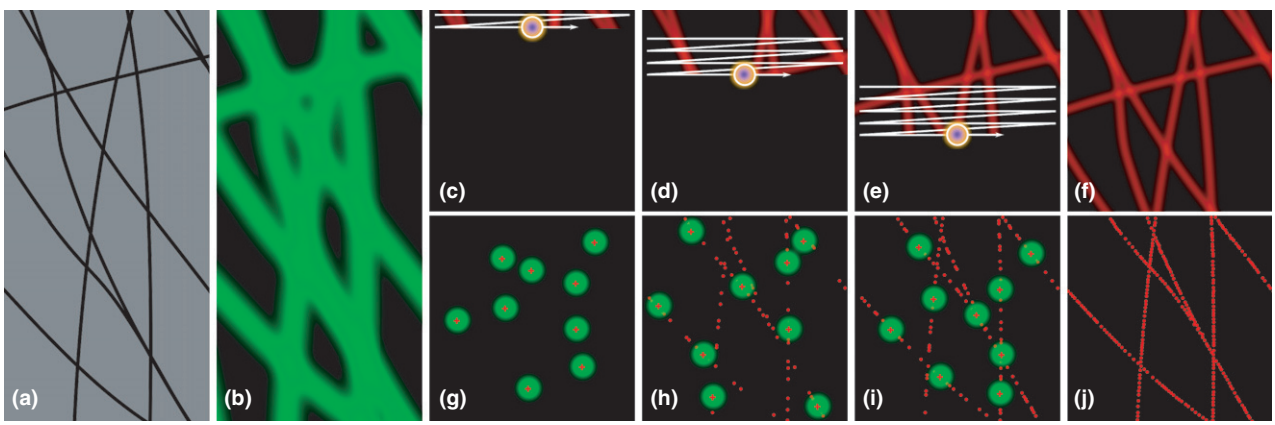

Fig. 1 Acquisition strategies in STORM and STED. (a) An artificially generated example of closely spaced filaments, which has features that are smaller than the optical diffraction limit, can be decorated with fluorophores at a very high density. (b) A simulation of the resulting diffraction limited image if all of the subsequent fluorophores are illuminated at the same time, as is the case with most conventional fluorescence microscopy approaches. (c–f) In STED, a sub-diffraction region is illuminated using two different sources. The first source (in blue) turns on all fluorophores within the white circle. The second source (in orange) is superimposed, and turns off the fluorophores in a region surrounding a small point. As a consequence, only fluorescence in the blue area visible in the figure is detected, while the fluorophores in the orange area are turned on and then immediately forced off. The excitation and STED beams are scanned across the sample to capture the image, as is done in confocal microscopy, to generate a super-resolution image. (g–j) In STORM, all of the fluorophores are maintained in an off-state using a combination of imaging buffers and illumination with an appropriate light source throughout imaging. A small subset of fluorophores is randomly turned on using a second light source, and imaged briefly before they return to the off-state. An image of the resulting structure is built up as different subsets of fluorophores turn on and off. (f and j) The underlying filaments can be visualized after the STED beam completes its scan or after sufficient numbers of fluorophores have been captured and localized using STORM.

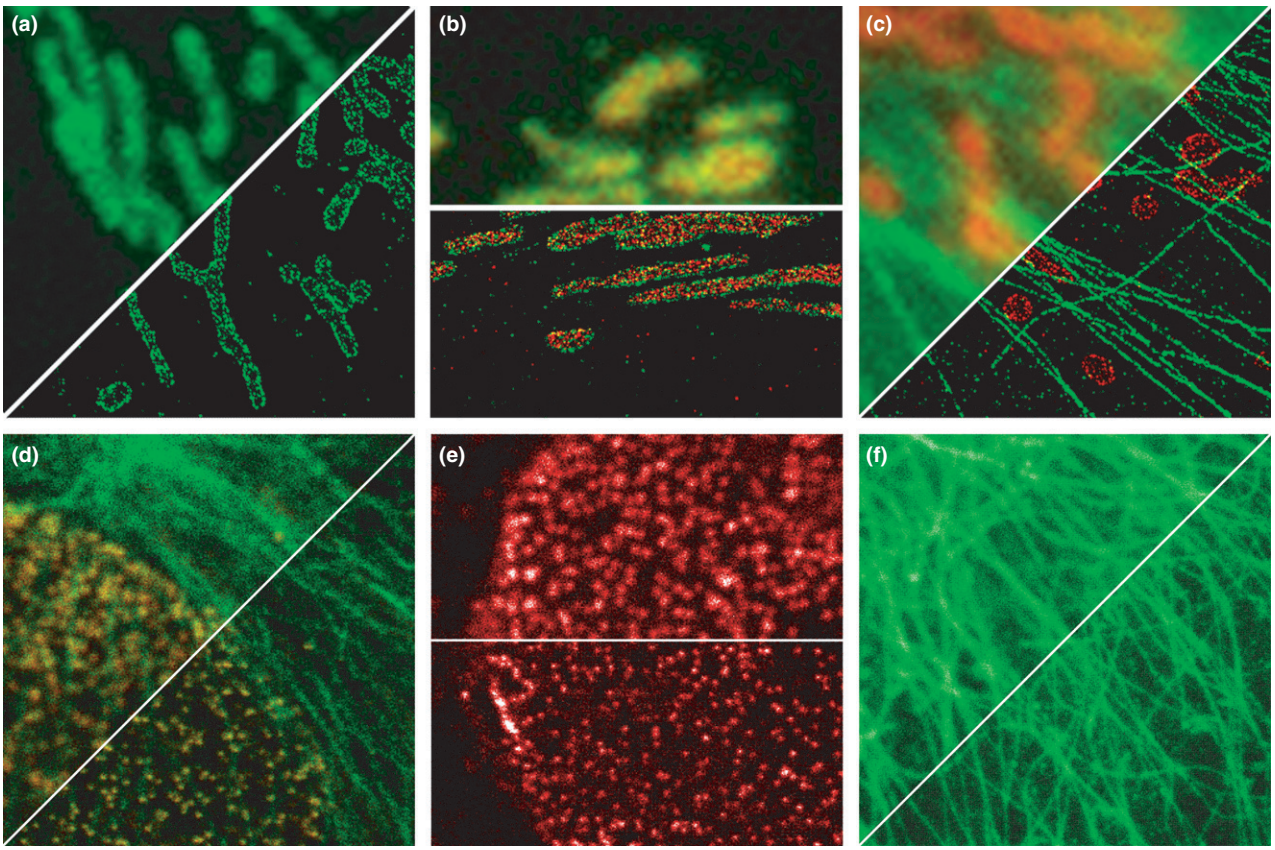

Fig. 2 Examples of STORM and STED images. Top row: STORM images of BS-C-1 cells. Conventional images were acquired using TIRF microscopy. (a and b) Mitochondrial proteins Tom20 (green) and ATP Synthase (red), which reside in the outer and inner mitochondrial membranes respectively. (c) Mitochondria protein Tom20 (red) and microtubules (green). Samples were prepared and imaged as described previously (Tam *et al.* 2014b). Bottom row: STED. (d–f) Multi-color STED images of PtK2 cells. Conventional images were acquired using confocal microscopy. In red, NUP135 has been tagged by means of STAR488, while in green Tubulin has been tagged using STAR440SX. Both of these dyes are from Abberior. All images are 10 × 10 μm in size.

combination of the overlapping blur induced by the diffraction limited image of each fluorescent molecule. In STORM, and in general in all of the SMLM techniques, fluorophores are imaged in a single-fluorophore regime (i.e. one molecule at a time). After the image of a single fluorophore (or in practice, a collection of non-overlapping images of individual fluorescent molecules) has been acquired, the localization of each fluorophore is determined by calculating with high precision the centroid of the fluorescent signal recorded from a single molecule. With each frame, a subset of localizations is generated. All of the successful localizations accumulated from many frames are then used to generate a final super-resolution image of the sample. Fundamentally, this process requires that fluorophores can be switched between fluorescent and non-fluorescent states (Patterson and Lippincott-Schwartz 2002; Fernández-Suárez and Ting 2008). This can be achieved in a number of different ways, giving way to the many different implementations of SMLM. For example, in PALM, this was first achieved using photoactivatable fluorescent proteins. In STORM a dye-pair approach was used in its first implementation (Rust *et al.* 2006; Bates *et al.* 2007). Two different fluorophores, which are referred to as the activator and reporter dyes, are conjugated onto an antibody. The reporter dye is responsible for the signal that generates the final image when excited by the imaging laser (Fig. 3a–c), and it is maintained in a non-fluorescent state through the use of an imaging buffer (see Sample preparation). To randomly activate the fluorescence of a small subset of non-overlapping reporter dye molecules, the activation laser in combination with the activator dye is needed. When the activator dyes on any given antibody receive sufficient stimulation from an activation laser (Fig. 3a–c; see Laser intensity), they can cause a neighboring reporter dye molecule to become fluorescent [typically if it is on the same secondary antibody, it is close enough to cause activation (Dempsey *et al.* 2009)]. The efficiency of the activation is governed by two main factors: first, the ratio of activator dyes to reporter dyes (there is an optimal ratio

for each pair of dyes, but generally, the number of activator dyes should be higher than the number of reporter dyes per antibody), and second, the intensity of the activation laser.

Once a subset of reporter dye molecules are activated, the imaging laser beam is turned on and acquisition starts. During acquisition, the intensity of the activation laser can be adjusted in order to increase or decrease the total number of randomly activated fluorophores. The imaging laser not only generates fluorescence signal, but it also causes any activated fluorophores to return to a non-fluorescent state. Therefore, a typical STORM imaging sequence consists of one frame in which the activation laser is turned on, randomly causing a small subset of dye-pairs to become fluorescent, followed by a series of frames in which the imaging laser is turned on, to image those dye-pairs that have become fluorescent while simultaneously causing those same dye-pairs to become non-fluorescent, restoring the initial state (Fig. 3a–c; see Image acquisition). This frame sequence is repeated until the desired number of localizations is achieved.

Aside from activator-reporter dye pairs, which are routinely used in STORM, particularly for multi-color STORM approaches (Bates *et al.* 2007; Huang *et al.* 2008a; Xu *et al.* 2013; Tam *et al.* 2014b), additional fluorophore options are now available (Dempsey *et al.* 2011; Oddone *et al.* 2014). As one illustrative example, conventional dyes such as MitoTracker Red, ER-Tracker Red, and LysoTracker Red have been used for STORM after the discovery that such dyes can be forced to photoswitch using a STORM image acquisition scheme (Shim *et al.* 2012). Although there are many options available, the dye-pair approach is most commonly attributed to STORM. Other implementations of SMLM have subtle variations from STORM with regards to the fluorophore type with which the technique is attributed to, or in the strategy for controlling the fluorescence signal. For example, in PALM microscopy, the fluorophores that are typically attributed to this technique are photoactivatable fluorescent proteins (PA-FP), which are expressed by the sample itself through transfection. Fluorescence is controlled by means of photoconversion or photoactivation, as opposed to photoswitching (e.g. dye pairs in STORM) (Fernández-Suárez and Ting 2008). In both dSTORM or GSDIM, conventionally available fluorophores are often used, which can be placed into a dark state (e.g. long-lived radical state or long-lived dark state) (Fölling *et al.* 2008; Heilemann *et al.* 2008). However, the acquisition strategy differs from STORM in that a single laser can be used which continuously illuminates the sample, and no activation laser is used.

STED is usually based on a confocal microscope. In the case of this configuration, the resolution is limited by the size of the spot at which the excitation beam is focused on the sample. The size of the spot is set by the diffraction limit. In STED microscopy, this limit is overcome by inhibiting fluorescence in the outer regions of the excitation spot. This effectively translates into a reduction of the fluorescent spot to a size that is below the diffraction limit, and as a direct consequence of this, the resolution of the system is increased beyond that limit. Fluorescence inhibition in STED microscopy is achieved by combining the excitation beam with a second one, called the depletion beam. It is essential that the wavelength of this depletion beam falls within the emission spectrum of the dye used. Light from the depletion beam interacts with the excited dye molecules by means of a mechanism called stimulated emission (Hell and Wichmann 1994; Klar and Hell 1999). This mechanism is the same one in which laser emission is based. In a fluorescent molecule, the energy of photons from the excitation beam is absorbed, promoting electrons in the molecule to excited states. After a certain time, these electrons will relax, and fall back to the ground state, emitting a fluorescence photon. These photons can have different wavelengths, which are distributed in a way that is characteristic of the dye molecule and is usually known as the emission spectra for that dye. When a depletion beam is superimposed to the excitation beam, stimulated emission can be triggered. As a result of this mechanism, in the presence of a depletion photon, an excited electron tends to relax, emitting a photon that replicates both the phase and wavelength of that particular depletion photon. In other words, by applying a depletion beam with a wavelength included in the emission spectrum of the dye, a preferred relaxation wavelength is introduced. If this beam intensity is above a certain value, called the saturation intensity, one can force practically all the excited electrons to relax at that wavelength. Downstream, a spectral filter can be used to reject photons at that wavelength. In short, this means that by applying a depletion beam above certain intensity, fluorescence can be switched off over controlled areas.

To reduce the size of the fluorescence spot on the sample, the depletion beam is focused onto a ring or donut shaped light distribution on top of the excitation spot. As explained previously, in the areas in which the depletion beam intensity is above the saturation intensity, fluorescence is inhibited by stimulated emission. Owing to the shape of the ring, this only happens in the outer parts of the excitation spot, and as a consequence, the diameter of the fluorescence spot is reduced, as depicted in Fig. 3f, and the resolution of the system is improved. Furthermore, increasing the overall intensity of the depletion beam reduces the central area of the ring where the intensity is below the saturation intensity. This translates into the well-known increase of resolution with depletion intensity in STED imaging, as shown in Fig. 3f. This is discussed in more detail in the Laser intensity section. There are several different methods that have been reported to generate a ring to switch off fluorescence in the outer area of the excitation spot (Klar *et al.* 2000, 2001). However, the most common method is to introduce a vortex phase mask into the beam path, as shown in Fig. 3e. This phase mask creates a phase singularity in the central point of the beam where intensity is zero, generating the desired ring around the

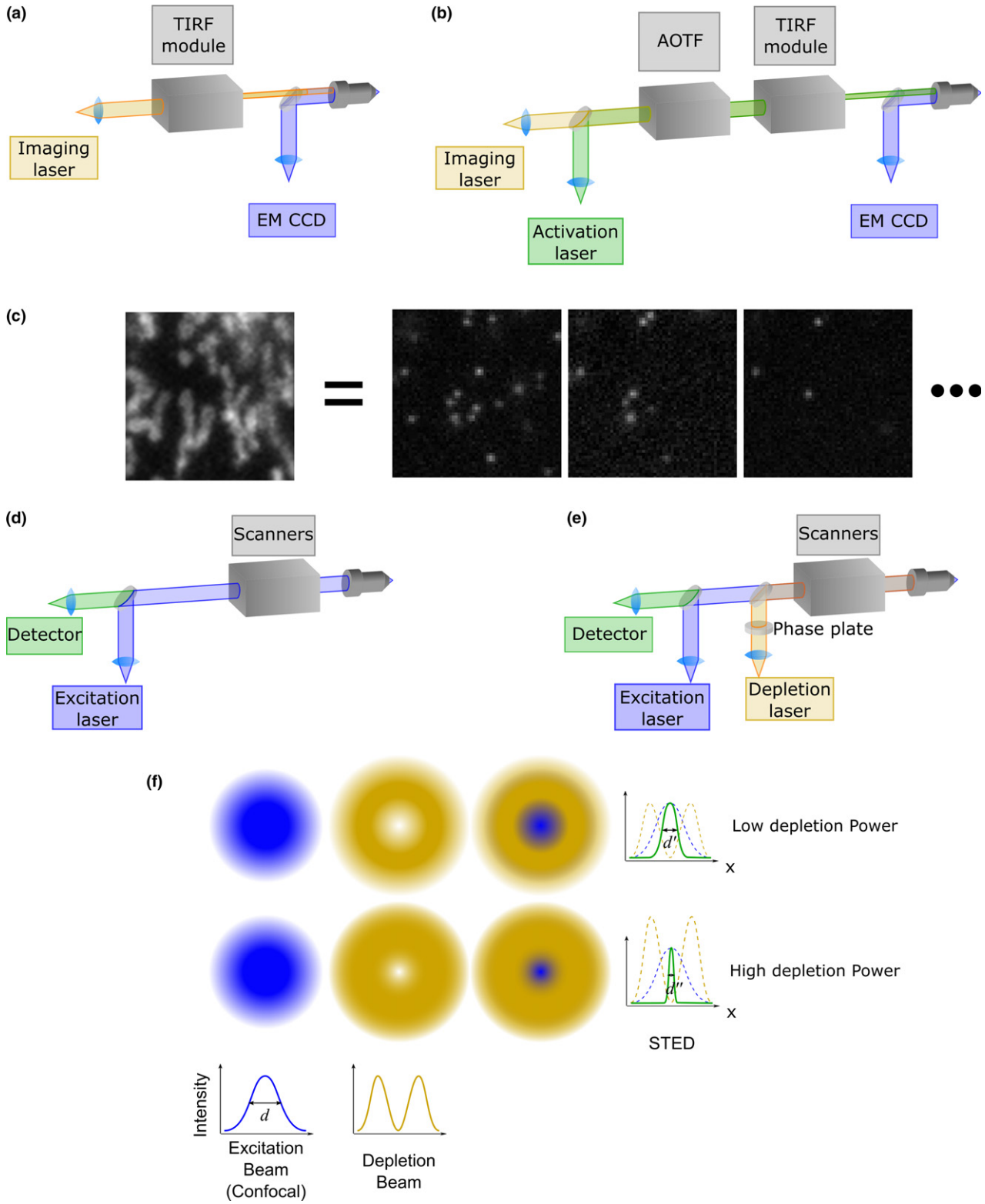

Fig. 3 Implementation of STORM and STED. (a) Sketch of a TIRF microscope. When the imaging laser is delivered to the sample, all fluorophores are excited. (b) In a typical TIRF-based STORM setup, one or more activation lasers are added along with an acousto-optic tunable filter (AOTF) to precisely control the timing of the laser pulses delivered to the sample. (c) When using the TIRF microscope shown in (a) to image mitochondria, the resulting image is the combination of the overlapping fluorescence from all fluorophores. In STORM, shown in (b), these overlapping fluorophores are separately imaged as single, non-overlapping fluorophores. In the activation step (not shown), the AOTF is used to deliver the activation laser to the sample, which activates the fluorescence of a small subset of the fluorophores. Next, the imaging laser is used to capture images of individual fluorophores (this same laser, in combination with the imaging buffer, turns off the fluorescence of the activated fluorophores). This three-frame sequence shows raw data acquired using the imaging laser. By the end of this sequence, most of the fluorophores are no longer active and therefore the cycle can be repeated. Tens of thousands of these frames are collected in a typical STORM experiment. (d) Sketch of a confocal setup and of a (e) STED setup. A depletion source is propagated through a phase plate that generates the donut shaped intensity distribution in the focus, and is overlaid to the excitation beam to raster scan the sample usually by means of the scanners. (f) Images of the excitation and depletion beams that are scanned over the sample, and the intensity curves that are related to them. The resolution of the confocal system is related to the width of the excitation beam, *d*. The combination of the excitation and depletion beams generates a narrower fluorescence spot, which is shown in green on the plots on the right. The width of the fluorescence spot is further reduced from *d'* to *d''* when increasing the depletion beam power.

excitation spot when the beam is focused on the sample (Török and Munro 2004).

Although fluorescence is inhibited in the outer area of the excitation spot, excitation/relaxation cycles continue to occur in the fluorescent molecules. Therefore, in STED microscopy the electrons that relax through stimulated emission will emit a photon, but this will not reach the detector. This translates in a decrease of the overall signal detected when compared to the confocal image acquired using the same excitation intensity. To obtain comparable fluorescence signal between confocal and STED images, the excitation beam intensity is commonly increased in the STED image acquisition process. Higher excitation intensities and fluorescence inhibition in the outer parts of the excitation beam usually combine to result in increased photobleaching. This should be definitely considered when using STED microscopy, and may be accounted for when preparing the sample, as will be described later.

Comparing STORM to STED, one of the advantages of STORM is that single fluorophores are being imaged, which is particularly important for quantitative imaging (i.e. when it is important to count the exact number of molecules in a given structure). However, an important possibility to consider is that the same fluorophore may become fluorescent more than once (e.g. through re-activation, or by blinking), which may lead to challenges for quantitative imaging. This challenge can be mitigated, as has been shown in both the PALM and STORM communities, enabling one to use PALM or STORM for quantitative imaging at the single-protein level (Durisic *et al.* 2012; Sengupta and Lippincott-Schwartz 2012). The efficiency of fluorophore cycling (i.e. number of times that a fluorophore is excited compared to the number of times that it is imaged) is better for STORM than for STED, since every cycle can potentially be captured in the case of STORM, whereas cycling occurs repeatedly without imaging in the depletion zone for STED. An important advantage of STED is the simplicity of controlling fluorophores, which can make it a more versatile option (fluorophore choice is not limited to those that can undergo photoswitching, photoconversion, or photoactivation; however, it is limited by depletion laser choice and availability, which will be discussed next).

Laser intensity

Generally, the laser powers needed for STORM are lower than those needed for STED, especially taking into consideration the fact that the laser beam is concentrated onto a small area in STED, as opposed to being distributed across the entire field in STORM. Although both STORM and STED utilize significantly higher laser intensities when compared to conventional microscopy (e.g. TIRF and confocal), the relatively lower laser intensities used for STORM may be an advantage for situations in which lower intensities are needed. This may be important for live cell imaging, where low laser intensities are usually desirable (Eggeling *et al.* 2013a; Lakadamyali 2014; Neupane *et al.* 2014). However, as in any live cell imaging application, there are many other aspects that should be considered as well, such as acquisition time, phototoxicity, viability, and more.

In STORM, it is important to set the laser intensities appropriately. In the dye-pair scenario described previously (see Fluorophore control), multiple lasers are needed. The imaging laser intensity (Fig. 3a–c) must be high enough to push any activated fluorophores back to the dark state, which also depends on the imaging buffer. The imaging laser intensity is usually fixed for the time-course of a STORM acquisition, with a typical value around ~1 kW/cm^2 at 647 nm (Tam *et al.* 2014b). In contrast, the activation laser intensity must be carefully controlled during the time-course of the experiment to set up an appropriate density of activated fluorophores. Initially, the imaging laser alone is able to activate a small subset of fluorophores, even in the absence of any light from the activation laser (Heilemann *et al.* 2008). However, over the acquisition time, the number of fluorophores which can be activated at a given activation laser intensity diminishes. Thus, the activation laser intensity

can be increased to raise the number of activated fluorophores. Proper control of the intensity of the activation laser can lead to higher quality STORM images. The intensity of the activation laser should be maintained at a level such that there are not too many activated fluorophore molecules to minimize overlap between neighboring activated fluorophores, but at the same time not too few of them so that the total acquisition time is not prolonged unnecessarily. If the intensity of the activation laser is increased too quickly, fluorophores can start to overlap, affecting the final quality of the STORM image. As an example, for an experiment in which the dye pair AlexaFluor 405-AlexaFluor 647 is imaged, initially the activation laser can remain off, but in the course the experiment its intensity is usually gradually increased, and by the end of the STORM acquisition, can be as high as ~ 20 W/cm^2.

As a side note, the timing of the delivery of laser light to the sample can also be adjusted to allow for longer or shorter amounts of time for the activated fluorophores to pass back to the dark state (e.g. by adjusting the number of frames between which the activation laser is delivered, or by adjusting the frame rate; see Fig. 3c). Therefore, to optimize fluorophore control, there is a critical balance in laser intensity, imaging buffer concentrations, and the timing of the laser light delivery.

In STED, high depletion laser intensities are needed to achieve optimal resolution. It has been shown that the resolution of a STED microscope depends on the ratio between the depletion beam intensity and the saturation intensity (which is the intensity of the depletion laser beam for which the population of the excited state drops by a factor of 1/e). As it is shown in Fig. 3f, as intensity of the depletion beam increases, the central area of the donut becomes reduced. This translates to the fact that resolution of a STED system increases with increasing intensity of the depletion beam (Westphal and Hell 2005). In theory, there is no limit to this statement, and resolution could be improved further and further just by increasing the depletion beam intensity. In practice, there are two factors that can limit the light intensity level that can be delivered to the sample. The first of these parameters is the amount of light that the sample can withstand. If the sample is not completely transparent, and there is some absorption of the depletion beam wavelength, then there is a limit to the intensity that can be delivered without damaging it. The second parameter is the maximum power that the depletion source itself can deliver.

Since the resolution of a STED system increases with the depletion beam intensity, laser sources with high powers are required. In the early implementations of the technique, femto second pulsed laser sources and optical parametric oscillators were used for their high peak intensities (Klar *et al.* 2001; Willig *et al.* 2006a). Since the depleting laser beam wavelength needs to fall within the emission spectrum of the fluorescent dye used, these sources used for STED microscopy limited the availability of suitable fluorescent dyes to those that emit in the infrared region of the spectrum. However, further developments allowed for the implementation of STED microscopy using diode lasers (Westphal *et al.* 2003a,b), supercontinuum sources (Auksorius *et al.* 2008; Wildanger *et al.* 2008), continuous wave laser sources (Willig *et al.* 2007), or even off-the-shelf mass-produced laser sources (Schrof *et al.* 2011). This growth in the availability of laser sources increased the number of fluorescent dyes that are suitable for STED microscopy. In fact, even green fluorescent protein (GFP), one of the most commonly used dyes for microscopy, has been used for STED imaging in both non-biological and biological samples (Willig *et al.* 2006b), as well as in multicellular organisms such as GFP-expressing C. Elegans (Rankin *et al.* 2011).

Recently, the use of gated detection has allowed for a significant reduction of the depletion intensity needed for STED imaging. In this approach, excitation is performed using a pulsed source, and depletion is usually performed by means of a continuous wave laser (Moffitt *et al.* 2011; Vicidomini *et al.* 2011), although implementations using a pulsed laser source for depletion have also been reported (Vicidomini *et al.* 2013). For detection, a photon counting device is used, which is able to determine the time at which each photon reaches the detector. Under these conditions, not only the number of photons detected can be determined, but also the time at which they are detected with respect to the excitation pulse. To generate super-resolution images, only those photons that have arrived to the detector during a particular range of time are considered in gated STED (gSTED). The principle behind this technique can be understood if it is considered that the depletion beam reduces the lifetime of electrons in the excited state, and therefore, photons detected at longer times after the excitation pulse are more likely to have been generated in the central part of the excitation point. An increase in the resolving power of the STED system has been reported using lower STED laser beam intensities by means of time gating, at expense of the intensity and the signal-to-background ratio (Vicidomini *et al.* 2011).

As explained earlier, high light intensity levels can have an impact on the sample itself. High light intensity levels can also accelerate photobleaching. These effects are important and should be considered for *in-vivo* applications, since they may affect the viability or normal function of living cells. Other implementations of RESOLFT, in which photoswitchable dyes are used, may be an alternative, since these implementations have allowed for a considerable reduction in the light levels required to achieve super-resolution, although longer settling times may also require longer acquisition times (Hofmann *et al.* 2005; Bossi *et al.* 2006).

Although STORM also requires quite high light power levels, these are spread over the whole field of view, and since every emitted photon is used for detection, in general

photobleaching and light intensities are less of a problem for STORM when compared to STED.

Microscope platform

One of the main differences between STORM and STED is the setup that is needed for their implementation. STORM usually utilizes a wide field microscope as a platform, whereas STED microscopy is usually based on a confocal configuration (Fig. 3).

Most STORM implementations are based on a wide field total internal reflectance fluorescence (TIRF) system (Fig. 3). In TIRF systems, a beam of laser light is introduced through the objective in an off-center location. This causes the light that illuminates the sample to exit the objective at an oblique angle. This angle can be adjusted by changing the distance that the beam is displaced from the optical axis of the objective. When the angle is set appropriately, total internal reflection occurs on the interface formed by the cover slip and the sample, and a thin evanescent wave reaches the sample which effectively restricts the fluorescence illumination to a thin region of the sample immediately adjacent to the glass surface (Axelrod 2001). TIRF systems are commercially available on most wide field microscopes. The advantages of using a TIRF-based STORM system are that, first, it is very cost-effective to implement, and second, it can achieve high signal to background ratios by restricting the illumination of light to a thin region near the surface of the glass coverslip. Although most STORM implementations are based on TIRF, it is important to note that TIRF is not a prerequisite for STORM. For example, the combination of a selective plane illumination microscopy microscope with SMLM has been demonstrated (Cella *et al.* 2011; Zhao *et al.* 2014).

As mentioned previously, a TIRF setup is not complicated to implement in a cost effective manner. The sample is illuminated by means of conventional laser sources to activate and inhibit the fluorophores. Images of the entire field of view are recorded at once on an electron-multiplying charge-coupled device camera. This needs to be synchronized with the illumination system, which can be done using an acousto-optic tunable filter. These additional pieces of hardware are commonly available. Although not an inherent property of STORM itself, the fact that TIRF is commonly utilized implies that STORM is particularly well-suited for imaging cell membranes and proteins situated near it. That said, by adjusting the angle of illumination to be near, but not at, TIRF, it is possible to use STORM to image structures that are located deeper inside the cell. Nevertheless, as a general rule of thumb for TIRF-based STORM systems, the closer the plane of focus is to the glass surface, the better the results will be; as the focal plane moves farther away from the glass surface, the overall background of the acquired images increases.

STED is usually based on a confocal setup. Although confocal microscopy is quite common, it may not be straightforward to modify a commercial confocal system to enhance it with STED capabilities. As mentioned previously, there are many different ways to generate a ring of light which is completely dark in the center (Klar *et al.* 2000, 2001; Török and Munro 2004). However, alignment between excitation and depletion beams is crucial for successful STED imaging. Aligning these two beams at the nanometric scale is a difficult task, and some solutions have been implemented to have them aligned by design (Wildanger *et al.* 2009a), or even autoaligned by means of adaptive optics (Gould *et al.* 2013).

Implementation of the scanning system may be complicated because of synchronization issues with the point detection unit. Although nowadays confocal systems can provide acquisition times close to video rate by using resonant scanning mirrors, raster scanning the field of view point by point can set a limitation to the temporal resolution that can be achieved by means of STED microscopy. However, recent developments have been reported in which scanning is parallelized, and several points of the field of view are scanned at once in the same system, reducing the scanning time and increasing the speed at which STED images can be generated (Bingen *et al.* 2011; Yang *et al.* 2014).

Finally, another critical point in the design of a STED system is the selection of both the excitation and depletion laser sources, which are usually quite specific, and, in general, costly. Since the depletion laser wavelength has to fall within the emission spectrum of the fluorescent molecule, the selection of the label of choice to use in the experiments is strictly related to the hardware available in the microscope. As mentioned previously in the Laser intensity section, it is desirable that depletion sources can provide high optical powers, and therefore it is ultimately the depletion source that sets a limit to the fluorescent molecules that can or cannot be used on a particular STED microscope.

Although STED systems are becoming more affordable nowadays, it is probably safe to say that implementation of a STORM system may be somehow simpler and more cost effective than a STED system.

Sample preparation

Sample preparation usually is very specific to the technique of choice, whether it is a super-resolution technique or not. In the case of SMLM techniques, there can be subtle differences depending on the type of fluorophore used.

As mentioned previously, the classical implementation of STORM utilizes photoswitchable dyes or fluorophores. When compared to STED, the availability of dyes for STORM is relatively limited. The dye-pair approach requires special protocols to conjugate fluorescent dyes to antibodies.

For fixed cells, immunostaining is typically performed, using a primary antibody against a target of interest, followed by a secondary antibody. This step may be time-consuming; however, integration of microfluidics with STORM may help to streamline sample preparation (Tam *et al.* 2014a). The secondary antibody is typically labeled with both an activator and a reporter dye (see Fluorophore control). However, new options for sample preparation are rapidly being developed, including the possibility of using Fab fragments or nanobodies (Ries *et al.* 2012). In addition, an increasing number of photoswitchable dyes is becoming available as applications of the technique are developed (Dempsey *et al.* 2011; Oddone *et al.* 2014), and in specific applications, commercially available dyes may even be used directly for STORM imaging (Shim *et al.* 2012).

An often overlooked consideration is that STORM samples are typically imaged in aqueous imaging buffers. The imaging buffer is critical for maintaining the fluorophores in a dark state (e.g. not fluorescent until activated). Typically, these buffers contain a reducing agent such as cysteamine or β-mercaptoethanol, along with an oxygen scavenger system (Dempsey *et al.* 2011). However, other options for STORM imaging buffers also exist (Vaughan *et al.* 2013). The use of an aqueous imaging buffer is a key difference between STORM and STED (STED samples can be imaged in a variety of different media; live samples are typically imaged in aqueous buffer, but fixed samples are typically mounted in mounting media).

Although there are differences between STORM and other SMLM techniques, with additional sample preparation modifications, some of the fluorophores which are used in other SMLM techniques may be suitable for imaging on a microscope that is designed for STORM (i.e. it may be possible to perform PALM imaging on a STORM microscope) (Fernández-Suárez and Ting 2008). The relationship of STORM to other SMLM techniques opens up additional possibilities for sample preparation. Regardless of whether dye-pairs or other fluorophores are selected, careful optimization of the sample preparation protocols is required for successful STORM imaging. In most cases, particular care is required in the areas of fixation and high-density fluorophore labeling. Improper fixation and immunostaining, which may not be relevant when imaging using conventional microscopes, may become apparent at increased resolution. In the case of live imaging, there are also many options for sample preparation (Fernández-Suárez and Ting 2008). These considerations might limit the applications for which STORM is a suitable technique.

In the case of STED, the only limit to the dyes that can be used is based on their emission spectrum. To achieve stimulated emission, the wavelength of the depletion source used must fall outside the excitation spectrum of the dye, but within its emission spectrum. It is also desirable that the wavelength of the depletion source does not coincide with the emission peak of the dye, and should be shifted toward longer wavelengths where emission is not so intense. Otherwise, most of the fluorescence would be rejected by the filter. However, when depletion wavelengths are close to the emission spectrum peak, STED efficiency increases, although the probability to excite fluorophores that have remained in the ground state also increases (Vicidomini *et al.* 2012). STED can be performed with a wide variety of dyes, which keeps growing with the new laser sources available for this technique. It is true, however, that the depletion sources available in a particular STED system will limit the dyes that can be used in that system according to the conditions detailed.

Other than choosing an appropriate dye for the specific STED system, sample preparation does not require specific protocols. However, it is desirable to follow necessary steps to reduce photobleaching, such as use of specific mounting media. This flexibility in sample preparation and dyes available for STED has enabled the technique to be applicable in-vivo (Fernández-Suárez and Ting 2008; Eggeling *et al.* 2013b; Neupane *et al.* 2014), since fluorescent proteins such as GFP can be used (Willig *et al.* 2006b), and acquisition times are reduced (see Image acquisition section).

Multi-color imaging can be performed using both modalities. The traditional way to perform multi-color STORM imaging is to take advantage of the fact that antibodies are labeled with both an activator and a reporter dye; by varying the activator dye while keeping the same reporter dye, additional colors can be acquired in a quasi-simultaneous manner (i.e. alternating cycles between the different colors) (Bates *et al.* 2007). However, as the number of colors increases, complexities may arise, such as cross-talk, fluorophore performance, imaging buffer, and imaging time (Tam *et al.* 2014b). Although there are a number of strategies for alleviating these complexities (Bates *et al.* 2007; Dempsey *et al.* 2011), one way to side-step all of these complexities is to use an approach for multi-color STORM based on sequential STORM imaging (Tam *et al.* 2014b).

The wide availability of dyes that are compatible with STED imaging has also allowed for multi-color STED imaging. There are two main approaches: one uses an excitation and depletion source for each dye, so that dyes with different emission spectra can be used (Donnert *et al.* 2007; Rankin *et al.* 2008). Another more cost effective approach to multi-color STED consists in selecting dyes that have similar emission spectra but different Stokes shifts, and therefore, different absorption maxima. These pairs of dyes are each excited with a different laser line, but can share the same depletion source. The acquisition strategy, then, is based on a sequential scheme, in which each color is generated separately. Lateral resolutions of ~40 nm were reported, imaging mitochondrion in mammalian cells (Schmidt *et al.* 2008). As in the case for traditional multi-color

STORM, it is important to ensure that the pairs of dyes are selected to minimize cross talk between them.

Image processing

STORM requires extensive image processing, which typically occurs after image acquisition. The image processing involves identification and localization of each fluorophore, followed by rendering of the resulting image. Identification usually requires that individual fluorophores are non-overlapping (i.e. only those fluorophores that are deemed to be high-quality images of isolated single fluorophores are marked for analysis). There are several methods for localization, but a common one uses a Gaussian as a model to approximate the point spread function; each identified fluorophore is fit to a Gaussian and the precise position of the central point of this Gaussian is recorded. The brighter the fluorophore, the more accurate the result of the localization will be. The total image processing time depends on the number of localizations being performed; any given STORM image may need between 100 000 and 10 000 000 localizations. In general, these image processing steps prevent immediate feedback on image quality and for inexperienced users this lack of immediate feedback can cause unexpected experimental failures. There are a growing number of different algorithms for processing STORM data, many of which help to alleviate this lag time. As an example, using a GPU-based implementation called GraspJ, it is possible to generate real-time STORM images to provide users with immediate feedback (Brede and Lakadamyali 2012).

One of the main advantages of STED is the fact that, just as in the case of confocal imaging, the images are available immediately after acquisition; no post processing is required. However, it is common to apply deconvolution routines on STED images, especially on those obtained by means of gSTED because of lower signal-to-noise ratios achieved. Considering that the acquisition time is on the order of seconds, or even lower if parallelized STED is used, as mentioned in Microscope platform section (Bingen *et al.* 2011), and that post processing is not strictly required, the throughput of STED microscopy is currently significantly higher than that of STORM. This feature is especially desirable for in-vivo applications.

Image acquisition

The acquisition process may be more difficult to optimize in a STORM system compared to a STED system. To generate a single STORM image, a large number of individual acquisitions need to be obtained (Fig. 3a–c). In the case of STORM, the acquisition process consists of a single activation frame (in which a small subset of fluorophores are brought from a dark state to an activated state), followed by a sequence of imaging frames (in which single fluorophore molecules are imaged and returned to the dark state). This procedure can be quite time consuming, often involving tens of thousands of frames for a high-quality STORM image (typically about 15–30 min for a single-color STORM image; longer for additional colors). Under these circumstances, it is necessary to take into account possible drift of the sample, because of the mechanical stability at the oil interface between sample and microscope objective, temperature changes, etc. That said, there are options to significantly decrease the acquisition time. Since the final image resolution is dependent on the total number of localizations, one way to reduce the acquisition time would be to reduce the total number of localizations. Thus, one can speed up acquisition time at the cost of image resolution (Jones *et al.* 2011). This is an important consideration for live-cell imaging. For example, live-cell imaging was demonstrated using PALM with spatial resolutions of approximately 60 nm and temporal resolutions on the order of 25 s (Shroff *et al.* 2008). If one were to image only single molecules, then it would be possible to achieve temporal resolutions on a millisecond time scale, as has been demonstrated in the PALM community (Manley *et al.* 2008). Single-particle tracking PALM (spt-PALM) can be used to study the mobility and trajectory of proteins in living cells and to generate statistics on populations of proteins (Niu and Yu 2008; Hoze *et al.* 2012). Generally, for live imaging of larger structures, the use of compressed sensing approaches (Zhu *et al.* 2012), or brighter fluorophores in combination with higher laser intensities can also lead to high-quality STORM images at fast acquisition speeds on the order of a few seconds with spatial resolutions up to 30 nm in the lateral direction and 50 nm in the axial direction, and temporal resolutions of 1–2 s (Jones *et al.* 2011).

In STED, the acquisition time is comparable to the case of confocal microscopy, and it is on the order of seconds. Acquisition time may be longer in STED compared to confocal because of lower signal to noise ratio or higher spatial sampling to correspond to higher resolution. As mentioned previously, acquisition speed in STED can be further increased by means of parallelization. Based on this inherent feature, STED microscopy is a great candidate for *in-vivo* imaging, where dynamics are important. The technique has been used to image several different types of samples. Of course, super-resolution has many applications for imaging subcellular structures, not only in fixed, but also in *in-vivo* samples. In this sort of applications, STED microscopy has been reported to achieve lateral resolutions of about 30 nm. The technique has been successfully used for imaging at a depth of 120 μm in living organotypic brain slices, with resolutions of 60-80 nm (Urban *et al.* 2011). These studies showed changes in actin-based structures inside spines and spine necks that could be modulated by neuronal activity. STED has also been combined with two photon microscopy (Moneron and Hell 2009; Bianchini

et al. 2012), and used for deep tissue imaging in mouse brain slices, showing that the technique is applicable even under conditions of high scattering media (Ding *et al.* 2009). In fact, STED has also been successfully applied for imaging neurons in the brain of a live mouse over extended periods of time with 70 nm resolution (Berning *et al.* 2012). STED has been also used to study molecular dynamics, and it has been successfully combined with fluorescence correlation spectroscopy in order to study single molecule dynamics in the nanoscale volumes in the plasma membrane of living cells (Kastrup *et al.* 2005; Eggeling *et al.* 2009; Ringemann *et al.* 2009).

In conclusion, although both STORM and STED are suitable for *in vivo* imaging applications, from the perspective of acquisition time, the inherent temporal resolution and flexibility in sample preparation of STED may be a clear advantage until fast STORM acquisition schemes become readily available.

Resolution

Although both STORM and STED can achieve super-resolution, the actual result depends on a number of factors. In STORM, the spatial resolution is determined by the probe size, labeling density, and localization precision. The use of primary and secondary antibodies for immunostaining can result in an effective probe size on the order of 10–15 nm, which can affect the perceived size of a nano-scale-sized object when imaged using STORM. As mentioned previously, resolutions of 10 nm in the lateral direction and 20 nm in the axial direction have been achieved using STORM in fixed cells (Xu *et al.* 2012). At this size scale, for certain applications, it may be important to apply alternate strategies for labeling structures based on smaller, 4–6 nm probes, such as nanobodies and Fab fragments (Ries *et al.* 2012). Probe size is a consideration for any fluorescence microscopy technique, but is an even more important consideration for super-resolution techniques. The labeling density can affect the image resolution as well, since STORM images are reconstructed point by point (Figs 1 and 3). If the number of localizations per area is not sufficiently high, the final image resolution will be reduced. Finally, as described previously, each of the individual fluorophores are individually localized. The precision of this localization contributes to the final resolution of the image. Although there are many parameters that determine localization precision (Stallinga and Rieger 2012), the most important parameter for localization precision is the number of photons collected per fluorophore. Generally, brighter fluorophores lead to better localization precision.

In the case of STED, as explained in previous sections, the resolution that can be achieved using this techinque is strongly related to the intensity of the depletion beam. If the laser source used can deliver high intensities and the sample can stand them, then the resolution of the technique can be pushed to its limit. This is the case of densely packed nitrogen-vacancy centers in diamond samples, that were shown in STED images with an unprecedented resolution of 5.8 nm resolution (Rittweger *et al.* 2009), which is the highest reported using this technique. However, selection of photons relaxing at specific lifetimes through gated detection, has allowed for increased resolution with lower depletion times (Vicidomini *et al.* 2013).

In terms of axial resolution, both STORM and STED have been extended to the third dimension. One of the

Table 1 Unique advantages and disadvantages of STORM and STED

STORM	STED
+Typically based on wide field TIRF microscopy. Therefore, systems are cost effective, and can potentially be implemented relatively easily by users familiar with optics	+Usually based on confocal microscopy. Although implementation can be costly and not straightforward, users familiar with confocal will find a commercial STED system easy to use
−TIRF mode works best near glass surface (works better with flatter cells)	+Good for imaging thicker samples because of confocal nature of system
−Lengthy acquisition, although new approaches reduce the acquisition time needed depending on the desired resolution	+Fast acquisition: Image can be available in a matter of seconds (easier to achieve higher temporal resolution)
−Extensive post-acquisition image processing is required to reconstruct image	+No post-acquisition image processing is required (super-resolution image immediately available)
−Samples can be prone to drift (this can be corrected in most cases)	+Higher throughput
+Fluorophore switching cycles are not wasted	−Fluorophores undergo a large number of forced on/off switches without contributing to the final image. This can lead to increased photobleaching that should be considered in the experiment
+Highest spatial resolution achievable to date (best case scenario)	+*In vivo* applications, where higher temporal resolution is needed (e.g. in living animals)
+Lower light levels compared to STED (more suitable for *in vivo* applications in which lower temporal resolution is acceptable)	−Higher light levels that may limit the samples that can be used (new modalities reduce these levels)

simplest and most cost-effective ways to implement 3D STORM imaging is to use an astigmatic lens, which can yield an axial resolution of 50-60 nm over a range of ~800 nm (Huang *et al.* 2008b). With the addition of a second objective, dual-objective STORM can improve the axial resolution to ~ 20 nm (however, the range over which images can be acquired is substantially reduced) (Xu *et al.* 2012). Effectively, the introduction of an astigmatic lens changes the point spread function of the microscope. An alternative approach, which is based on changing the point spread function to a double helix, can also be used for three dimensional imaging (Pavani *et al.* 2009). The trade-off for these point spread function approaches is that the size of the image of each individual single fluorophore has to be increased (i.e. more camera pixels need to be used to capture each individual fluorophore). In order to reach the desired number of localizations, this typically results in longer acquisition times (since individual fluorophores have to be spaced further apart to minimize overlap). Dual-objective geometries, which have been used in PALM, might also lead to higher axial resolutions, up to 10 nm (Shtengel *et al.* 2009). The trade-off of dual-objective techniques is that samples have to be prepared in a manner that allows for objectives to approach the sample from both directions (thick samples may not perform well). Finally, multi-focal imaging, in which multiple focal planes are captured simultaneously, can also be used for three dimensional imaging (Juette *et al.* 2008). The trade-off of multi-focal techniques is that the overall intensity signal must be split across the different focal planes (particularly problematic for weaker signals).

STED has been extended to the z direction, with an improvement in resolution in the axial direction. To do so, the depleting beam is divided, and two different phase masks are used. One of the masks is the vortex phase plate, described previously, while the second one is a top-hat phase mask. After each of the beams is propagated through the corresponding phase plate they're recombined, and focused onto the sample. The beam traveling through the second phase mask generates two foci of light above and below the focal plane. When this is combined with the ring generated by the vortex phase plate, a dark volume is generated that is surrounded by light in every direction in the space (Harke *et al.* 2008; Han *et al.* 2009). Lower depletion laser intensities required for gSTED have allowed for more efficient implementations of this concept, since the power of the depleting light source needs to be divided into two different paths. An axial resolution of ~100 nm has been reported using this method in a biological sample (Wildanger *et al.* 2009b). However, by combining STED and 4Pi microscopy, and collecting fluorescence through two different microscope objectives, axial and lateral resolutions of ~ 45 nm have been achieved in biological samples (Schmidt *et al.* 2008). Finally, STED has been combined with adaptive optics in an effort to reduce the effect of the aberrations introduced by the sample and increasing its performance, especially in the case of 3D imaging (Gould *et al.* 2012), and also to provide a robust method to align the system (Gould *et al.* 2013).

Summary and conclusions

STORM and STED are two super-resolution techniques based on two different fundamental strategies to control fluorescence. STORM is based on random, massively parallelized switching of individual fluorophores, whereas STED relies on controlled pumping of fluorophores between fluorescent and non-fluorescent (depleted) states.

Overall, STORM has reported the highest resolutions to date on an optical imaging system, and has proven its utility in many different biological problems. Although STED images have not reported such high resolutions in biological applications, the wide variety of dyes compatible with the technique, and relatively simple and fast acquisition process, make this technique suitable for *in-vivo* applications. Furthermore, the advances in gSTED, which have allowed for the reduction of the depletion beam intensity needed may reduce the impact of imaging on living samples. The unique advantages and disadvantages of STORM and STED are summarized in Table 1.

In conclusion, the rise of super-resolution imaging modalities such as STORM and STED has led to exciting new possibilities. Both STORM and STED are great candidates to reveal the mysteries of the nanoscale world.

Acknowledgments and conflict of interest disclosure

The authors would like to thank the Whitaker International Fellows and Scholars Program, the ICFO Super-resolution Nanoscopy Facility (SLN), and the Nikon Center of Excellence in STORM at ICFO.

All experiments were conducted in compliance with the ARRIVE guidelines. The authors have no conflict of interest to declare.

References

Agard D. A. (1984) Optical sectioning microscopy: cellular architecture in three dimensions. *Annu. Rev. Biophys. Bioeng.* **13**, 191–219.

Auksorius E., Boruah B. R., Dunsby C., Lanigan P. M. P., Kennedy G., Neil M. A. A. and French P. M. W. (2008) Stimulated emission depletion microscopy with a supercontinuum source and fluorescence lifetime imaging. *Opt. Lett.* **33**, 113.

Axelrod D. (2001) Total internal reflection fluorescence microscopy in cell biology. *Traffic* **2**, 764–774.

Bailey B., Farkas D. L., Taylor D. L. and Lanni F. (1993) Enhancement of axial resolution in fluorescence microscopy by standing-wave excitation. *Nature* **366**, 44–48.

Bates M., Huang B., Dempsey G. T. and Zhuang X. (2007) Multicolor super-resolution imaging with photo-switchable fluorescent probes. *Science* **317**, 1749–1753.

Berning S., Willig K. I., Steffens H., Dibaj P. and Hell S. W. (2012) Nanoscopy in a living mouse brain. *Science* **335**, 551.

Betzig E., Lewis A., Harootunian A., Isaacson M. and Kratschmer E. (1986) Near field scanning optical microscopy (NSOM). *Biophys. J.* **49**, 269–279.

Betzig E., Isaacson M., Barshatzky H., Lewis A. and Lin K. (1988) Near-field scanning optical microscopy (NSOM), in *Proc. SPIE*, **0897**, pp. 91–99.

Betzig E., Patterson G. H., Sougrat R., Lindwasser O. W., Olenych S., Bonifacino J. S., Davidson M. W., Lippincott-Schwartz J. and Hess H. F. (2006) Imaging intracellular fluorescent proteins at nanometer resolution. *Science* **313**, 1642–1645.

Bianchini P., Harke B., Galiani S., Vicidomini G. and Diaspro A. (2012) Single-wavelength two-photon excitation-stimulated emission depletion (SW2PE-STED) superresolution imaging. *Proc. Natl Acad. Sci.* **109**, 6390–6393.

Bingen P., Reuss M., Engelhardt J. and Hell S. W. (2011) Parallelized STED fluorescence nanoscopy. *Opt. Express* **19**, 23716.

Binnig G., Quate C. and Gerber C. (1986) Atomic force microscope. *Phys. Rev. Lett.* **56**, 930–933.

Bossi M., Fölling J., Dyba M., Westphal V. and Hell S. W. (2006) Breaking the diffraction resolution barrier in far-field microscopy by molecular optical bistability. *New J. Phys.* **8**, 275.

Brede N. and Lakadamyali M. (2012) GraspJ: an open source, real-time analysis package for super-resolution imaging. *Opt. Nano.* **1**, 1–7.

Cella Zanacchi F., Lavagnino Z., Perrone Donnorso M., Del Bue A., Furia L., Faretta M. and Diaspro A. (2011) Live-cell 3D super-resolution imaging in thick biological samples. *Nat. Meth.* **8**, 1047–1049.

Dempsey G. T., Bates M., Kowtoniuk W. E., Liu D. R., Tsien R. Y. and Zhuang X. (2009) Photoswitching mechanism of cyanine dyes. *J. Am. Chem. Soc.* **131**, 18192–18193.

Dempsey G. T., Vaughan J. C., Chen K. H., Bates M. and Zhuang X. (2011) Evaluation of fluorophores for optimal performance in localization-based super-resolution imaging. *Nat. Meth.* **8**, 1027–1036.

Ding J. B., Takasaki K. T. and Sabatini B. L. (2009) Supraresolution imaging in brain slices using stimulated-emission depletion two-photon laser scanning microscopy. *Neuron* **63**, 429–437.

Donnert G. (2006) Macromolecular-scale resolution in biological fluorescence microscopy. *Proc. Natl Acad. Sci.* **103**, 11440–11445.

Donnert G., Keller J., Wurm C. A., Rizzoli S. O., Westphal V., Schönle A., Jahn R., Jakobs S., Eggeling C. and Hell S. W. (2007) Two-color far-field fluorescence nanoscopy. *Biophys. J.* **92**, L67–L69.

Durisic N., Godin A. G., Wever C. M., Heyes C. D., Lakadamyali M. and Dent J. A. (2012) Stoichiometry of the human glycine receptor revealed by direct subunit counting. *J. Neurosci.* **32**, 12915–12920.

Eggeling C., Ringemann C., Medda R., *et al.* (2009) Direct observation of the nanoscale dynamics of membrane lipids in a living cell. *Nature* **457**, 1159–1162.

Eggeling C., Willig K. I. and Barrantes F. J. (2013) STED microscopy of living cells - new frontiers in membrane and neurobiology. *J. Neurochem.* **126**, 203–212.

Fernández-Suárez M. and Ting A. Y. (2008) Fluorescent probes for super-resolution imaging in living cells. *Nat. Rev. Mol. Cell Biol.* **9**, 929–943.

Fölling J., Bossi M., Bock H., Medda R., Wurm C. A., Hein B., Jakobs S., Eggeling C. and Hell S. W. (2008) Fluorescence nanoscopy by ground-state depletion and single-molecule return. *Nat. Meth.* **5**, 943–945.

Gould T. J., Burke D., Bewersdorf J. and Booth M. J. (2012) Adaptive optics enables 3D STED microscopy in aberrating specimens. *Opt. Express* **20**, 20998.

Gould T. J., Kromann E. B., Burke D., Booth M. J. and Bewersdorf J. (2013) Auto-aligning stimulated emission depletion microscope using adaptive optics. *Opt. Lett.* **38**, 1860.

Gustafsson M. G. L. (2000) Surpassing the lateral resolution limit by a factor of two using structured illumination microscopy. *J. Microsc.* **198**, 82–87.

Gustafsson M. G. L. (2005) Nonlinear structured-illumination microscopy: wide-field fluorescence imaging with theoretically unlimited resolution. *PNAS* **102**, 13081–13086.

Gustafsson M. G., Agard D. A. and Sedat J. W. (1999) I5M: 3D widefield light microscopy with better than 100 nm axial resolution. *J. Microsc.* **195**, 10–16.

Han K. Y., Willig K. I., Rittweger E., Jelezko F., Eggeling C. and Hell S. W. (2009) Three-dimensional stimulated emission depletion microscopy of nitrogen-vacancy centers in diamond using continuous-wave light. *Nano Lett.* **9**, 3323–3329.

Harke B., Keller J., Ullal C. K., Westphal V., Schönle A. and Hell S. W. (2008) Resolution scaling in STED microscopy. *Opt. Express* **16**, 4154.

Hayat M. A. (1974) Principles and techniques of scanning electron microscopy. *Bio. App.* **1**. xiv+273.

Heilemann M., vande Linde S., Schüttpelz M., Kasper R., Seefeldt B., Mukherjee A., Tinnefeld P. and Sauer M. (2008) Subdiffraction-resolution fluorescence imaging with conventional fluorescent probes. *Angew. Chem. Int. Ed.* **47**, 6172–6176.

Hell S. W. (2003) Toward fluorescence nanoscopy. *Nat. Biotechnol.* **21**, 1347–1355.

Hell S. W. (2004) Strategy for far-field optical imaging and writing without diffraction limit. *Phys. Lett. A* **326**, 140–145.

Hell S. W. (2007) Far-field optical nanoscopy. *Science* **316**, 1153–1158.

Hell S. W. (2009) Microscopy and its focal switch. *Nat. Methods* **6**, 24–32.

Hell S. W. and Kroug M. (1995) Ground-state-depletion fluorescence microscopy: a concept for breaking the diffraction resolution limit. *Appl. Phys. B* **60**, 495–497.

Hell S. and Stelzer E. H. K. (1992) Properties of a 4Pi confocal fluorescence microscope. *J. Opt. Soc. Am. A* **9**, 2159.

Hell S. W. and Wichmann J. (1994) Breaking the diffraction resolution limit by stimulated emission: stimulated-emission-depletion fluorescence microscopy. *Opt. Lett.* **19**, 780.

Hell S. W., Dyba M. and Jakobs S. (2004) Concepts for nanoscale resolution in fluorescence microscopy. *Curr. Opin. Neurobiol.* **14**, 599–609.

Hess S. T., Girirajan T. P. K. and Mason M. D. (2006) Ultra-high resolution imaging by fluorescence photoactivation localization microscopy. *Biophys. J .* **91**, 4258–4272.

Hofmann M., Eggeling C., Jakobs S. and Hell S. W. (2005) Breaking the diffraction barrier in fluorescence microscopy at low light intensities by using reversibly photoswitchable proteins. *Proc. Natl Acad. Sci.* **102**, 17565–17569.

Hoze N., Nair D., Hosy E., Sieben C., Manley S., Herrmann A., Sibarita J.-B., Choquet D. and Holcman D. (2012) Heterogeneity of AMPA receptor trafficking and molecular interactions revealed by superresolution analysis of live cell imaging. *PNAS* **109**, 17052–17057.

Huang B., Jones S. A., Brandenburg B. and Zhuang X. (2008a) Whole-cell 3D STORM reveals interactions between cellular structures with nanometer-scale resolution. *Nat. Meth.* **5**, 1047–1052.

Huang B., Wang W., Bates M. and Zhuang X. (2008b) Three-dimensional super-resolution imaging by stochastic optical reconstruction microscopy. *Science* **319**, 810–813.

Jones S. A., Shim S.-H., He J. and Zhuang X. (2011) Fast, three-dimensional super-resolution imaging of live cells. *Nat. Meth.* **8**, 499–505.

Juette M. F., Gould T. J., Lessard M. D., Mlodzianoski M. J., Nagpure B. S., Bennett B. T., Hess S. T. and Bewersdorf J. (2008) Three-dimensional sub–100 nm resolution fluorescence microscopy of thick samples. *Nat. Methods* **5**, 527–529.

Kastrup L., Blom H., Eggeling C. and Hell S. W. (2005) Fluorescence fluctuation spectroscopy in subdiffraction focal volumes. *Phys. Rev. Lett.* **94**, 178104.

Klar T. A. and Hell S. W. (1999) Subdiffraction resolution in far-field fluorescence microscopy. *Opt. Lett.* **24**, 954.

Klar T. A., Jakobs S., Dyba M., Egner A. and Hell S. W. (2000) Fluorescence microscopy with diffraction resolution barrier broken by stimulated emission. *Proc. Natl Acad. Sci.* **97**, 8206–8210.

Klar T., Engel E. and Hell S. (2001) Breaking Abbe's diffraction resolution limit in fluorescence microscopy with stimulated emission depletion beams of various shapes. *Phys. Rev.* **E 64**, 066613.

Kumar A., Wu Y., Christensen R., *et al.* (2014) Dual-view plane illumination microscopy for rapid and spatially isotropic imaging. *Nat. Protocols* **9**, 2555–2573.

Lakadamyali M. (2014) Super-resolution microscopy: going live and going fast. *Chemphyschem* **15**, 630–636.

Manley S., Gillette J. M., Patterson G. H., Shroff H., Hess H. F., Betzig E. and Lippincott-Schwartz J. (2008) High-density mapping of single-molecule trajectories with photoactivated localization microscopy. *Nat. Methods* **5**, 155–157.

Minsky M. (1988) Memoir on inventing the confocal scanning microscope. *Scanning* **10**, 128–139.

Moffitt J. R., Osseforth C. and Michaelis J. (2011) Time-gating improves the spatial resolution of STED microscopy. *Opt. Express* **19**, 4242.

Moneron G. and Hell S. W. (2009) Two-photon excitation STED microscopy. *Opt. Express* **17**, 14567.

Neupane B., Ligler F. S. and Wang G. (2014) Review of recent developments in stimulated emission depletion microscopy: applications on cell imaging. *J. Biomed. Optics* **19**, 080901.

Niu L. and Yu J. (2008) Investigating intracellular dynamics of FtsZ cytoskeleton with photoactivation single-molecule tracking. *Biophys. J .* **95**, 2009–2016.

Oddone A., Vilanova I. V., Tam J. and Lakadamyali M. (2014) Super-resolution imaging with stochastic single-molecule localization: concepts, technical developments, and biological applications. *Microsc. Res. Tech.* **77**, 502–509.

Patterson G. H. and Lippincott-Schwartz J. (2002) A photoactivatable GFP for selective photolabeling of proteins and cells. *Science* **297**, 1873–1877.

Pavani S. R. P., Thompson M. A., Biteen J. S., Lord S. J., Liu N., Twieg R. J., Piestun R. and Moerner W. E. (2009) Three-dimensional, single-molecule fluorescence imaging beyond the diffraction limit by using a double-helix point spread function. *Proc. Natl Acad. Sci.* **106**, 2995–2999.

Rankin B. R., Kellner R. R. and Hell S. W. (2008) Stimulated-emission-depletion microscopy with a multicolor stimulated-Raman-scattering light source. *Opt. Lett.* **33**, 2491.

Rankin B. R., Moneron G., Wurm C. A., Nelson J. C., Walter A., Schwarzer D., Schroeder J., Colón-Ramos D. A. and Hell S. W. (2011) Nanoscopy in a living multicellular organism expressing GFP. *Biophys. J .* **100**, L63–L65.

Ries J., Kaplan C., Platonova E., Eghlidi H. and Ewers H. (2012) A simple, versatile method for GFP-based super-resolution microscopy via nanobodies. *Nat. Meth.* **9**, 582–584.

Ringemann C., Harke B., vonMiddendorff C., Medda R., Honigmann A., Wagner R., Leutenegger M., Schönle A., W Hell S. and Eggeling C. (2009) Exploring single-molecule dynamics with fluorescence nanoscopy. *New J. Phys.* **11**, 103054.

Rittweger E., Han K. Y., Irvine S. E., Eggeling C. and Hell S. W. (2009) STED microscopy reveals crystal colour centres with nanometric resolution. *Nat. Photonics* **3**, 144–147.

Rust M. J., Bates M. and Zhuang X. (2006) Sub-diffraction-limit imaging by stochastic optical reconstruction microscopy (STORM). *Nat. Meth.* **3**, 793–796.

Schmidt R., Wurm C. A., Jakobs S., Engelhardt J., Egner A. and Hell S. W. (2008) Spherical nanosized focal spot unravels the interior of cells. *Nat. Methods* **5**, 539–544.

Schrof S., Staudt T., Rittweger E., Wittenmayer N., Dresbach T., Engelhardt J. and Hell S. W. (2011) STED nanoscopy with mass-produced laser diodes. *Opt. Express* **19**, 8066.

Sengupta P. and Lippincott-Schwartz J. (2012) Quantitative analysis of photoactivated localization microscopy (PALM) datasets using pair-correlation analysis. *BioEssays* **34**, 396–405.

Shim S.-H., Xia C., Zhong G., Babcock H. P., Vaughan J. C., Huang B., Wang X., Xu C., Bi G.-Q. and Zhuang X. (2012) Super-resolution fluorescence imaging of organelles in live cells with photoswitchable membrane probes. *PNAS* **109**, 13978–13983.

Shroff H., Galbraith C. G., Galbraith J. A. and Betzig E. (2008) Live-cell photoactivated localization microscopy of nanoscale adhesion dynamics. *Nat. Meth.* **5**, 417–423.

Shtengel G., Galbraith J. A., Galbraith C. G., *et al.* (2009) Interferometric fluorescent super-resolution microscopy resolves 3D cellular ultrastructure. *Proc. Natl Acad. Sci.* **106**, 3125–3130.

Siedentopf H. and Zsigmondy R. (1902) Uber Sichtbarmachung und Größenbestimmung ultramikoskopischer Teilchen, mit besonderer Anwendung auf Goldrubingläser. *Ann. Phys.* **315**, 1–39.

Stallinga S. and Rieger B. (2012) The effect of background on localization uncertainty in single emitter imaging, in *2012 9th IEEE International Symposium on Biomedical Imaging (ISBI)*, pp. 988–991. IEEE, Barcelona.

Stelzer E. H. K., Lindek S., Albrecht S., Pick R., Ritter G., Salmon N. J. and Stricker R. (1995) A new tool for the observation of embryos and other large specimens: confocal theta fluorescence microscopy. *J. Microsc.* **179**, 1–10.

Tam J., Cordier G. A., Bálint Š., Sandoval Álvarez Á., Borbely J. S. and Lakadamyali M. (2014a) A microfluidic platform for correlative live-cell and super-resolution microscopy. *PLoS ONE* **9**, e115512.

Tam J., Cordier G. A., Borbely J. S., Sandoval Álvarez Á. and Lakadamyali M. (2014b) Cross-talk-free multi-color STORM imaging using a single fluorophore. *PLoS ONE* **9**, e101772.

Török P. and Munro P. R. T. (2004) The use of gauss-laguerre vector beams in STED microscopy. *Opt. Express* **12**, 3605.

Urban N. T., Willig K. I., Hell S. W. and Nägerl U. V. (2011) STED nanoscopy of actin dynamics in synapses deep inside living brain slices. *Biophys. J .* **101**, 1277–1284.

Vaughan J. C., Dempsey G. T., Sun E. and Zhuang X. (2013) Phosphine quenching of cyanine dyes as a versatile tool for fluorescence microscopy. *J. Am. Chem. Soc.* **135**, 1197–1200.

Vicidomini G., Moneron G., Han K. Y., Westphal V., Ta H., Reuss M., Engelhardt J., Eggeling C. and Hell S. W. (2011) Sharper low-power STED nanoscopy by time gating. *Nat. Methods* **8**, 571–573.

Vicidomini G., Moneron G., Eggeling C., Rittweger E. and Hell S. W. (2012) STED with wavelengths closer to the emission maximum. *Opt. Express* **20**, 5225.

Vicidomini G., Schönle A., Ta H., Han K. Y., Moneron G., Eggeling C. and Hell S. W. (2013) STED nanoscopy with time-gated detection: theoretical and experimental aspects. *PLoS ONE* **8**, e54421.

Voie A. H., Burns D. H. and Spelman F. A. (1993) Orthogonal-plane fluorescence optical sectioning: three-dimensional imaging of macroscopic biological specimens. *J. Microsc.* **170**, 229–236.

Webb R. H. (1996) Confocal optical microscopy. *Rep. Prog. Phys.* **59**, 427–471.

Westphal V. and Hell S. (2005) Nanoscale resolution in the focal plane of an optical microscope. *Phys. Rev. Lett.* **94**, 143903.

Westphal V., Blanca C. M., Dyba M., Kastrup L. and Hell S. W. (2003a) Laser-diode-stimulated emission depletion microscopy. *Appl. Phys. Lett.* **82**, 3125.

Westphal V., Kastrup L. and Hell S. W. (2003b) Lateral resolution of 28 nm (λ/25) in far-field fluorescence microscopy. *Appl. Phys. B* **77**, 377–380.

Wildanger D., Rittweger E., Kastrup L. and Hell S. W. (2008) STED microscopy with a supercontinuum laser source. *Opt. Express* **16**, 9614.

Wildanger D., Bückers J., Westphal V., Hell S. W. and Kastrup L. (2009a) A STED microscope aligned by design. *Opt. Express* **17**, 16100.

Wildanger D., Medda R., Kastrup L. and Hell S. W. (2009b) A compact STED microscope providing 3D nanoscale resolution. *J. Microsc.* **236**, 35–43.

Willig K. I., Keller J., Bossi M. and Hell S. W. (2006a) STED microscopy resolves nanoparticle assemblies. *New J. Phys.* **8**, 106.

Willig K. I., Kellner R. R., Medda R., Hein B., Jakobs S. and Hell S. W. (2006b) Nanoscale resolution in GFP-based microscopy. *Nat. Methods* **3**, 721–723.

Willig K. I., Harke B., Medda R. and Hell S. W. (2007) STED microscopy with continuous wave beams. *Nat. Methods* **4**, 915–918.

Xu K., Babcock H. P. and Zhuang X. (2012) Dual-objective STORM reveals three-dimensional filament organization in the actin cytoskeleton. *Nat. Meth.* **9**, 185–188.

Xu K., Zhong G. and Zhuang X. (2013) Actin, spectrin, and associated proteins form a periodic cytoskeletal structure in axons. *Science* **339**, 452–456.

Yang B., Przybilla F., Mestre M., Trebbia J.-B. and Lounis B. (2014) Large parallelization of STED nanoscopy using optical lattices. *Opt. Express* **22**, 5581.

Zhao Z. W., Roy R., Gebhardt J. C. M., Suter D. M., Chapman A. R. and Xie X. S. (2014) Spatial organization of RNA polymerase II inside a mammalian cell nucleus revealed by reflected light-sheet superresolution microscopy. *PNAS* **111**, 681–686.

Zhu L., Zhang W., Elnatan D. and Huang B. (2012) Faster STORM using compressed sensing. *Nat. Meth.* **9**, 721–723.